Molecular simulation of orthobaric isochoric heat capacities near the critical point

Richard J. Sadus*
Centre for Computational Innovations, Swinburne University of Technology, P.O. Box 218 Hawthorn, Victoria 3122, Australia

(Received 9 July 2018; published 23 January 2019)

A molecular simulation strategy is investigated for detecting the divergence of the isochoric heat capacity (C_V) on the vapor and liquid coexistence branches of a fluid near the critical point. The procedure is applied to the empirical Lennard-Jones potential and accurate state-of-the-art *ab initio* two-body and two-body + three-body potentials for argon. Simulations with the Lennard-Jones potential predict the divergence of C_V, and the phenomenon is also observed for both two-body and two-body + three body potentials. The potentials also correctly predict the crossover between vapor and liquid C_V values and the subcritical liquid C_V minimum, which marks the commencement C_V divergence. The effect of three-body interactions is to delay the onset of divergence to higher subcritical temperatures.

DOI: 10.1103/PhysRevE.99.012139

I. INTRODUCTION

The critical point is reached when all of the physical properties of coexisting phases become identical [1,2]. For one-component fluids there is a unique critical point between vapor and liquid phases, whereas two-component fluids can exhibit both vapor-liquid and liquid-liquid critical points for a range of different compositions. In two-component fluids, the critical points form distinct critical lines that can be used to classify the different types of phase behavior [3]. A critical surface can be envisaged for three-component fluids [1]. The most common critical point involves only two phases, but tricritical points involving three phases and other higher order critical phenomena [4] are possible.

From a theoretical perspective, it has been established [5–7] that some key thermodynamic properties, such as the isochoric heat capacity (C_V) diverge at the critical point, i.e., $C_V \to \infty$ as $T \to T_c$, $p \to p_c$, $\rho \to \rho_c$, $x \to x_c$, where T, p, ρ, and x denote temperature, pressure, density, and composition (for mixtures), respectively, and the c subscript indicates a critical property. This behavior has also been observed from experimental data [8], including experiments in microgravity [9]. Recently, some theoretical studies [10–12] for one-component systems have suggested that thermodynamic properties do not diverge at a single critical point, but this alternative perspective is not widely accepted [13,14].

Molecular simulation [15] is usually the preferred theoretical method for evaluating statistical mechanical properties because it can be used to both rigorously and unambiguously determine the behavior of a specified intermolecular potential. However, issues such as the correlation length and finite size effects mean that it is difficult to apply to critical phenomena. Special finite size scaling algorithms [16,17] have been developed for phase behavior in the vicinity of the critical point. However, computational procedures are invariably designed to yield finite values and divergences are often only detected indirectly as computing failures.

Even if the weaknesses of the molecular simulation approach at the critical point could be addressed fully, it would not be easy to observe $C_V \to \infty$ because of the way that C_V is calculated from ensemble fluctuations. This work addresses this issue, demonstrating the usefulness of an alternative approach and reporting results from empirical, semiempirical, and *ab initio* two-body and three-body intermolecular potentials.

II. THEORY

A. Calculation of C_V from statistical ensembles

For the microcanonical (*NVE*), canonical (*NVT*), and grand canonical (μVT) ensembles, we obtain [15]

$$C_{V(NVE)} = \frac{1}{\frac{2}{3Nk}\left(1 - \frac{2\langle \delta E_{\rm pot}^2 \rangle}{3Nk^2\langle T^2\rangle}\right)}$$

$$C_{V(NVT)} = \frac{\langle \delta E_{\rm pot}^2 \rangle}{kT^2} + \frac{3Nk}{2}$$

$$C_{V(\mu VT)} = \frac{3Nk}{2} + \frac{1}{kT^2}\left(\langle \delta E_{\rm pot}^2 \rangle - \frac{\langle \delta E \delta N \rangle^2}{\langle \delta N^2 \rangle}\right), \quad (1)$$

where the angled brackets denote ensemble averages, N is the number of particles, T is the temperature, V is the volume, μ is the chemical potential, E is the total energy, $E_{\rm pot}$ is the potential energy, and k is Boltzmann's constant. In Eq. (1), δ denotes a fluctuation from the ensemble average, e.g., $\delta N^2 = N^2 - \langle N^2 \rangle$. The nature of these ensemble definitions means that it would be difficult to observe $C_V \to \infty$. It would require the fluctuations in either $E_{\rm pot}$ or N to be infinite for the *NVT* and μVT ensembles, which is very unlikely to occur in a conventional molecular simulation. Irrespective of the fluctuations in $E_{\rm pot}$, it is impossible to observe $C_V \to \infty$ from the above *NVE* ensemble definition.

*rsadus@swin.edu.au

Lustig [18–20] has proposed alternative methods for obtaining thermodynamic quantities from ensemble averages, which do not require fluctuation formulas. Molecular dynamics (MD) in the *NVE* ensemble normally also conserves total linear momentum (**P**) and, as such, is more accurately described as a *NVE***P** ensemble. Lustig [18] identified that the *NVE***P** ensemble also conserved another quantity (**G**) related to the motion of the particles. This insight permits the calculation of thermodynamic quantities, without using fluctuation formulas. C_V for the *NVE***PG** ensemble is given by

$$C_{V(NVEPG)} = \frac{k}{\Omega}, \tag{2}$$

where

$$\begin{aligned} \Omega &= 1 - \Omega_{00}\Omega_{20} \\ \Omega_{00} &= \frac{2}{3N-3}\langle K \rangle \\ \Omega_{20} &= -\left[1 - \frac{3N-3}{2}\right]\langle K^{-1} \rangle \end{aligned} \tag{3}$$

and K is the kinetic energy. It is evident from Eq. (2) that $C_V \to \infty$ means $\Omega \to 0$, which is computationally much easier to both evaluate and monitor.

B. Intermolecular potentials

The energy of interaction $[u(r)]$ between particles as a function of distance (r) can be simply obtained using the Lennard-Jones (LJ) potential [21],

$$u(r) = 4\varepsilon\left[\left(\frac{\sigma}{r}\right)^{12} - \left(\frac{\sigma}{r}\right)^{6}\right], \tag{4}$$

where σ and ε are the collision diameter and minimum well depth, respectively. The origin of the LJ potential is mainly empirical. It is an effective multibody potential, which is not specific to any atom, although it is widely believed to be most suitable for noble gases, such as argon.

In contrast, accurate *ab initio* two-body potentials have been developed specifically for argon. Jäger, Hellmann, Bich, and Vogel (JHBV) developed [22] an *ab initio* potential for argon using a modified version of the Tang-Toennies [23] function,

$$\begin{aligned} u_{\mathrm{JHBV}} &= A\exp(a_1 R + a_2 R^2 + a_{-1}R^{-1} + a_{-2}R^{-2}) - \sum_{n=3}^{8} f_{2n}(bR)\frac{C_{2n}}{R^{2n}} \\ f_{2n}(x) &= 1 - e^{-x}\sum_{k=0}^{2n}\frac{x^k}{k!}, \end{aligned} \tag{5}$$

where $R = r/\sigma$, $\varepsilon/k = 143.123$ K, and $\sigma = 0.336$ nm. The remaining terms are constants required to obtain optimal agreement with the energy curve and are given elsewhere [22].

Patkowski and Szalewicz (PS) reported [24] an *ab initio* pair interaction potential for argon, using basis sets with higher cardinal numbers. The attractive contribution was fitted to the same function as the JHBV potential, but the repulsive term is different, i.e.,

$$\begin{aligned} u_{\mathrm{PS}} &= (A + BR + CR^{-1} + DR^2 + ER^3)e^{-\alpha R} - \sum_{n=3}^{8} f_{2n}(bR)\frac{C_{2n}}{R^{2n}} \\ u_{\mathrm{PS}}^{\mathrm{sr}} &= (\tilde{A} + \tilde{B}R + \tilde{C}R^{-1} + \tilde{D}R^2)e^{-\tilde{\alpha}R - \tilde{\beta}R^2} \quad \text{for} \quad R < 0.387, \end{aligned} \tag{6}$$

for which $\varepsilon/k = 142.944$ K and $\sigma = 0.336$ nm. The meaning and values of the remaining parameters are the same as reported elsewhere [24].

It is of interest to contrast these *ab initio* potentials with the semiempirical potential for argon reported by Barker, Fisher, and Watts (BFW) [25]. The BFW potential was designed to fit solid, liquid, and gas data by combining the Barker-Pompe (u_{BP}) [26] and Bobetic-Barker (u_{BB}) [27] potentials,

$$u_{\mathrm{BFW}} = 0.75u_{\mathrm{BB}} + 0.25u_{\mathrm{BP}}, \tag{7}$$

which have the same analytical form, but different parameterization. The overall expression for the BFW potential is

$$\frac{u_{\mathrm{BFW}}}{\varepsilon} = \sum_{i=0}^{5} A_i(R-1)^i e^{\alpha(1-R)} - \sum_{n=6,8,10}\frac{C_n}{\delta + R^n}, \tag{8}$$

where $R = r/r_{\mathrm{min}}$ and r_{min} defines the interatomic separation at which the potential has a minimum. The characteristic parameters of the BFW potential for argon are $\varepsilon/k = 142.095$ K with its position at $r_{\mathrm{min}} = 0.376$ nm. The values of the other coefficients are as summarized in the literature [25].

The LJ potential incorporates the effective multibody contributions required for the calculation of thermodynamic properties and fluid phase equilibria. In contrast, the two-body potentials will often require additional higher-body terms to improve their accuracy. It has been well established [28–31] that the addition of the Axilrod-Teller-Muto (ATM) [32,33] three-body term is often sufficient:

$$u_{\mathrm{ATM}} = \frac{\nu(1 + 3\cos\theta_i\cos\theta_j\cos\theta_k)}{(r_{ij}r_{jk}r_{ik})^3}, \tag{9}$$

where ν is the nonadditive coefficient, which can be determined experimentally [34] from dipole oscillator strengths.

TABLE I. Summary of literature values [35–39] of the orthobaric densities for the Lennard-Jones potential and corresponding Ω and isochoric heat capacity data obtained in this work from *NVE***PG** MD simulations with $N = 2000$ particles.

T^*	ρ^* (Liquid)	$N\Omega$ (Liquid)	C_V (Liquid) J mol^{-1} K^{-1}	ρ^* (Vapor)	$N\Omega$ (Vapor)	C_V (Vapor) J mol^{-1} K^{-1}
0.75	0.819	0.400	20.8	0.00350	0.650	12.8
0.8	0.801	0.411	20.2	0.00591	0.640	13.0
0.833	0.786	0.418	19.9	0.00807	0.631	13.2
0.909	0.752	0.436	19.1	0.0151	0.620	13.4
1.0	0.704	0.462	18.0	0.0284	0.595	14.0
1.08	0.658	0.478	17.4	0.0480	0.558	14.9
1.15	0.630	0.486	17.1	0.068	0.536	15.5
1.2	0.560	0.484	17.2	0.099	0.503	16.5
1.24	0.523	0.483	17.2	0.124	0.472	17.6
1.25	0.516	0.472	17.6	0.148	0.454	18.3
1.27	0.496	0.476	17.5	0.178	0.418	19.9

For argon, $\nu = 7.3382 \times 10^{-90}$ J cm^9 [34]. The angles and separations in Eq. (9) refer to a triangular configuration of atoms. Combining Eq. (9) with the two-body potentials yields JBHV + ATM, PS + ATM, and BFW + ATM potentials.

C. Simulation details

We performed MD simulations in the *NVE***PG** ensemble [18,19] to determine Ω for the LJ potential along saturated vapor and liquid densities [35–39]. The *NVE***PG** ensemble simulations involve implementing a conventional *NVE***P** simulation while keeping track of the volume derivatives of the intermolecular potential and K. The initial configuration for all simulations was a face centered cubic lattice structure. The equations of motion were integrated using a five-value Gear predictor-corrector scheme [15] with a reduced time step of $\tau = 0.001$. A total of $N = 2000$ particles was used. For each state point, simulation trajectories were commonly run for 2×10^6 time steps with 1×10^6 time steps used to equilibrate the system. The cutoff radius was half of the box length and long-range corrections were applied. To calculate the standard error, the postequilibration data were divided into 10 equal blocks. The calculated standard errors are typically either less than or slightly larger than the size of the symbols used in the figures and, as such, are not shown. It will often be convenient to use reduced temperature ($T^* = kT/\varepsilon = \Omega_{00}/\varepsilon$) and reduced density ($\rho^* = \rho\sigma^3$). In contrast to T and ρ, which can only be evaluated from the specified intermolecular parameters, $C_V = kC_V^*$.

III. RESULTS AND DISCUSSION

We have specifically chosen to determine Ω along the saturated (orthobaric) liquid and vapor densities because many well-documented state points are available from either potential-based simulations [35–39] or experimental [8] studies. This means we can have confidence in the trend in Ω values. In contrast, calculating Ω along either the critical isochor or critical temperature is likely to have greater uncertainty because it would depend on the accuracy of the single critical datum point. Except for the LJ potential, which has been studied extensively [17], the critical point predicted by the potentials studied here has not been determined accurately. The orthobaric densities used for the LJ calculations are summarized in Table I.

The variation of Ω with respect to T^* along the saturated vapor and liquid curves of the LJ fluid is illustrated in Fig. 1 and the numerical values are summarized in Table I. The saturated vapor Ω values decline with increasing T^*. The rate of decline of the vapor phase Ω increases with increasing T^* and it is likely that $\Omega \to 0$ as $T^* \to T^*_c$, which means that $C_V \to \infty$ as $T^* \to T^*_c$. This is in contrast to other works [10–12], which failed to detect the divergence of C_V. In contrast to the vapor phase, the saturated liquid Ω values initially increase with increasing T^*. At $T^* \geqslant 1.15$, Ω appears to attain a maximum value, followed by lower values as $T^* \to T^*_c$. The liquid values appear to cross the vapor values, which is usually indicative of C_V divergence in real fluids, as discussed below. It is also likely that $\Omega \to 0$ ($C_V \to \infty$) as $T^* \to T^*_c$, for the liquid branch, although the evidence is not as compelling.

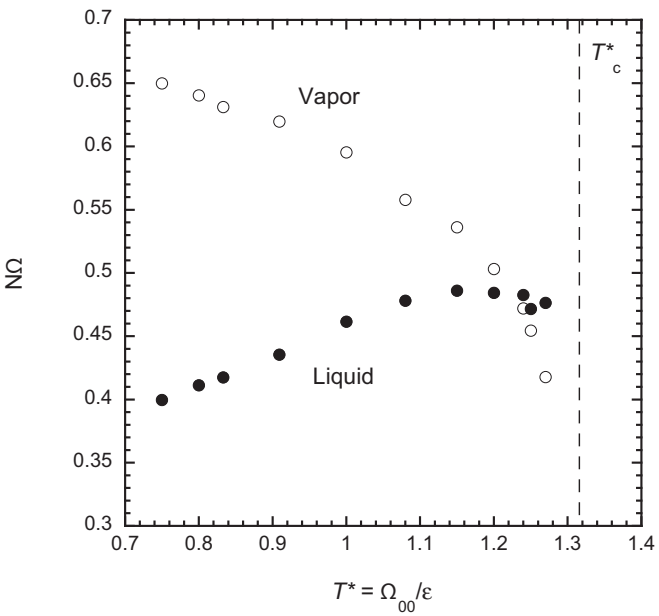

FIG. 1. The variation of Ω with respect to temperature along the coexisting vapor (○) and liquid (●) phases of the LJ potential ($N = 2000$) showing divergence when approaching the critical temperature (marked by a dashed line).

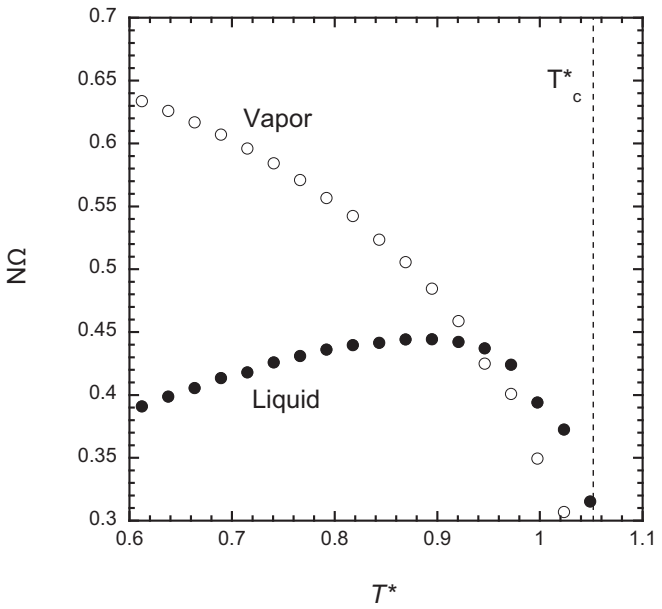

FIG. 2. The variation of Ω with respect to temperature along the coexisting vapor (○) and liquid (●) phases of the two-body JHBV potential for argon ($N = 500$) showing divergence in the vicinity of the critical temperature (marked by a dashed line). The maximum in the liquid Ω value corresponds to a C_V minimum.

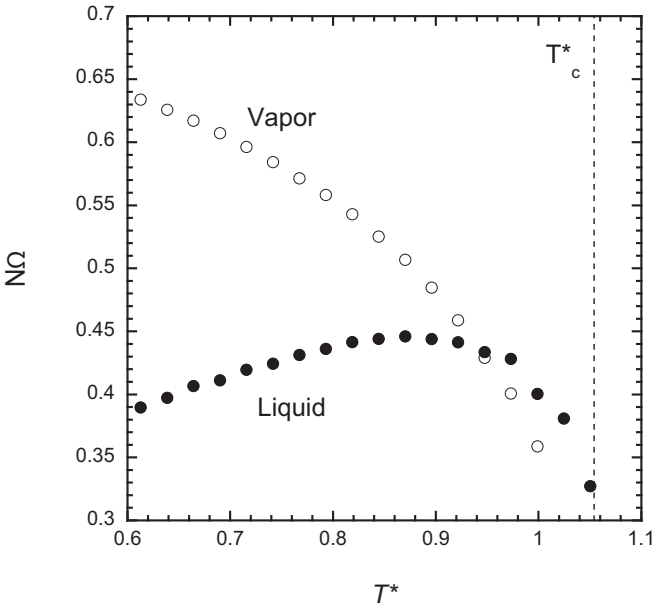

FIG. 3. The variation of Ω with respect to temperature along the coexisting vapor (○) and liquid (●) phases of the two-body PS potential for argon ($N = 500$), showing divergence in the vicinity of the critical temperature (marked by a dashed line). The maximum in the liquid Ω value corresponds to a C_V minimum.

Recently, orthobaric C_V simulation data [40] for argon potentials using Lustig's approach for the *NVT* ensemble [21] have been reported. The principle of equivalence [15,41] between statistical ensembles means these data can be analyzed to yield values of Ω. Results for the JHBV, PS, and BFW potentials are illustrated in Figs. 2–4.

Figure 2 shows that vapor Ω values obtained for the JHBV potential decline with increasing T^*. Significantly, as $T^* \rightarrow T^*_c$, the rate of this decline increases, providing a clear indication that $\Omega \rightarrow 0$. For the orthobaric liquid, Ω initially increases with increasing T^*, passing through a maximum value before rapidly diverging to lower values as $T^* \rightarrow T^*_c$. Therefore, we can infer that $\Omega \rightarrow 0$ as $T^* \rightarrow T^*_c$ for both the vapor and liquid phases. Figure 2 shows that the vapor and liquid phase Ω values cross in the vicinity of T^*_c. This is consistent with experimental C_V vapor and liquid values [8], which also cross before diverging. Qualitatively identical behavior was also observed for the *ab initio* PS (Fig. 3) and semiempirical BFW (Fig. 4) two-body potentials for argon. It is of particular interest to note that the semiempirical BFW potential yields similar results to the more recent *ab initio* JHBV and PS two-body potentials.

It is apparent from Figs 2–4 that the two-body potentials clearly display the crossover of Ω values and $\Omega \rightarrow 0$ as $T^* \rightarrow T^*_c$ for both the liquid and vapor phases. Comparing Figs 2–4 to Fig. 1 suggests a possible phenomenological explanation for the failure of some LJ potential simulations to correctly predict the divergence of C_V. The onset of C_V divergence is linked to the crossover of the liquid and vapor phase properties. For the JHBV, PS, and BFW potentials, both the maximum in the liquid phase Ω (C_V minimum) and crossover of the liquid and vapor curves occurred well before T^*_c. In contrast, for the LJ potential (Fig. 1), the crossover behavior occurs at values of T^* that are noticeably closer to T^*_c. The near-critical region is challenging for conventional simulations, which means that calculations for the LJ potential are arguably more prone to error because of the greater

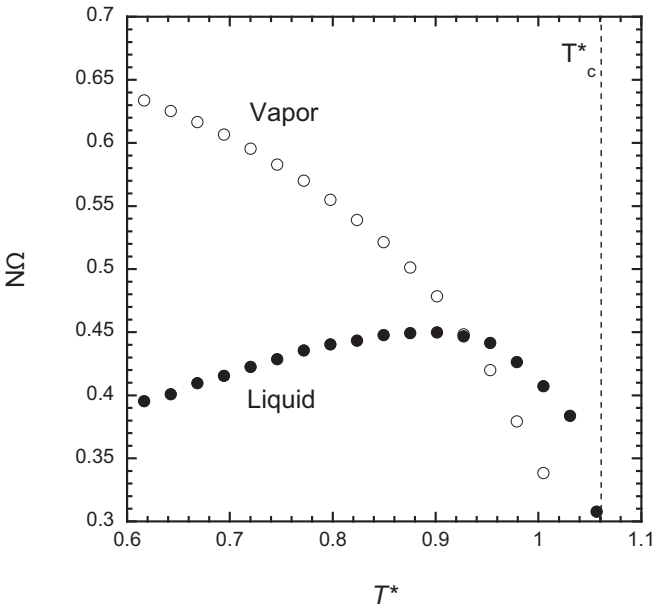

FIG. 4. The variation of Ω with respect to temperature along the coexisting vapor (○) and liquid (●) phases of the two-body BFW potential for argon ($N = 500$), showing divergence in the vicinity of the critical temperature (marked by a dashed line). The maximum in the liquid Ω value corresponds to a C_V minimum.

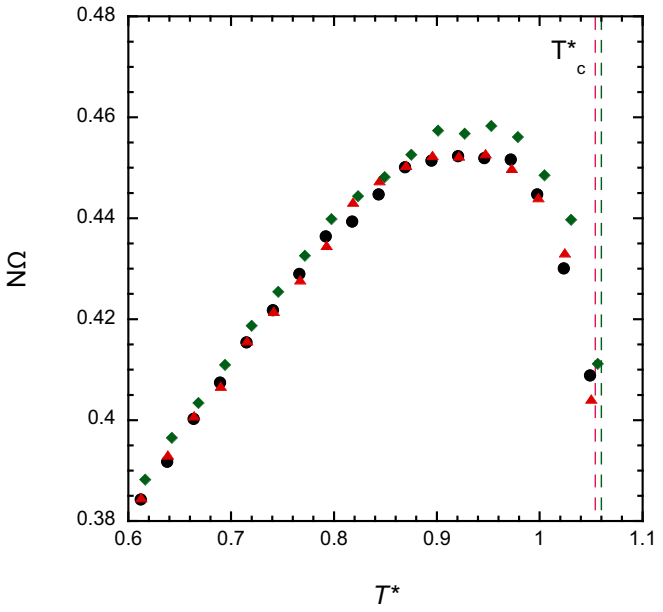

FIG. 5. The variation of Ω with respect to temperature along the coexisting liquid phase for the JHBV + ATM (●), PS + ATM (▲), and BFW + ATM (◆) potentials for argon ($N = 500$), showing divergence in the vicinity of the critical temperature (the different dashed lines reflect differences in ε values for the potentials). The maximum in the liquid Ω value corresponds to a C_V minimum.

proximity of this phenomenon to the critical point. The incorrect near-critical behavior of some LJ potential calculations may be caused by the failure to detect the liquid phase Ω maximum (C_V minimum) at subcritical temperatures. Our method does not exhibit these limitations.

The LJ potential is an effective multibody potential, whereas the JBHV, PS, and BFW potentials only consider two-body interactions. To investigate whether the absence of higher-body contributions was a factor in the results, we extended the analysis to include ATM interactions reported elsewhere [40]. The liquid Ω values as a function of T^* for the JHBV + ATM, PS + ATM, and BFW + ATM potentials are illustrated in Fig. 5. It is apparent that the results for JHBV + ATM and PS + ATM potentials are quantitatively similar for most temperatures, whereas the BFW + ATM potential predicts a higher Ω maximum than the other potentials. In common with the two-body calculations, in all cases a maximum Ω is observed, following which $\Omega \to 0$ as $T^* \to T^*_c$.

The addition of the ATM potential to the two-body potentials (Fig. 5) increases the Ω maximum, which occurs at higher T^*. The LJ potential (Fig. 1) also yields a larger Ω maximum for the liquid phase than the two-body potentials (Figs. 2–4). This means that the crossover between the liquid and vapor phase Ω values will most likely occur at a higher subcritical temperature than is observed for the two-body potentials.

IV. CONCLUSIONS

Calculating the Ω values is an effective method for detecting the divergence of C_V in the vicinity of the critical point. MD simulations with the LJ potential indicate C_V divergence, particularly along the saturated vapor curve. The behavior is also observed for both the saturated vapor and liquid phase Ω values obtained from accurate two-body JHBV, PS, and BFW potentials for argon. This is also the case when ATM interactions are added to the two-body potentials.

Calculations with the two-body and two-body + ATM potentials also correctly predict other experimentally observed subcritical phenomena such as the crossover of vapor and liquid C_V values and the C_V minimum. These observations were made for simulations with a relatively small number of particles. In other computational methods, such a small number of particles would be considered too few to permit definitive conclusions for properties near the critical point. Our approach does not appear to suffer from this limitation.

The inability of some approaches to correctly predicted the C_V behavior of the LJ potential near the critical point can be partly attributed to the crossover between liquid and vapor phase properties occurring relatively closer to the critical point, which causes well-documented computational difficulties for conventional simulations. In contrast, the crossover of C_V for accurate two-body potentials commences at noticeably lower subcritical temperatures. The effect of three-body interactions is to shift the C_V crossover closer to the critical temperature.

[1] R. J. Sadus, *High Pressure Phase Behaviour of Multicomponent Fluid Mixtures* (Elsevier, Amsterdam, 1992).
[2] R. J. Sadus, AIChE J. **40**, 1376 (1994).
[3] P. H. van Konynenburg and R. L. Scott, Philos. Trans. R. Soc. A (London) **298**, 495 (1980).
[4] R. J. Sadus, J. Phys. Chem. **96**, 5197 (1992).
[5] M. E. Fisher, in *Critical Phenomena*, edited by F. J. W. Hahne, Lecture Notes in Physics (Springer, Berlin, 1982), Vol. 186, pp. 1–139.
[6] M. E. Fisher, Rev. Mod. Phys. **70**, 653 (1998).
[7] H. Behnejad, J. V. Sengers, and M. A. Anisimov, in *Applied Thermodynamics of Fluids*, edited by A. R. H. Goodwin, J. V. Sengers, and C. J. Peters (RSC, Cambridge, 2010), pp. 321–367.
[8] E. W. Lemmon, M. O. McLinden, and D. Friend, in *NIST Chemistry WebBook, NIST Standard Reference Database Number 69*, edited by P. J. Linstrom and W. G. Mallard (National Institute of Standards and Technology, Gaithersburg, 2016).
[9] A. Haupt and J. Straub, Phys. Rev. E **59**, 1795 (1999).
[10] L. V. Woodcock, Int. J.Thermophys. **35**, 1770 (2014).
[11] L. V. Woodcock, Entropy **20**, 22 (2018).
[12] S. Pieprzyk, A. C. Brańka, Sz. Maćkowiak, and D. M. Heyes, J. Chem. Phys. **148**, 114505 (2018).
[13] J. V. Sengers and M. A. Anisimov, Int. J. Thermophys. **36**, 3001 (2015).
[14] I. H. Umirazkov, Int. J. Thermophys. **38**, 8 (2018).
[15] R. J. Sadus, *Molecular Simulation of Fluids: Theory, Algorithms and Object-Orientation* (Elsevier, Amsterdam, 1999).

[16] N. B. Wilding, Phys. Rev. E **52**, 602 (1995).
[17] J. J. Potoff and A. Z. Panagiotopoulos, J. Chem. Phys. **109**, 10914 (1998).
[18] R. Lustig, J. Chem. Phys. **100**, 3048 (1994).
[19] K. Meier and S. Kabelac, J. Chem. Phys. **124**, 064104 (2006).
[20] R. Lustig, Mol. Simul. **37**, 457 (2011).
[21] J. E. Jones, Proc. R. Soc. London, Ser. A **106**, 463 (1924).
[22] B. Jäger, R. Hellmann, E. Bich, and E. Vogel, Mol. Phys. **107**, 2181 (2009).
[23] K. T. Tang and J. P. Toennies, J. Chem. Phys. **80**, 3726 (1984).
[24] K. Patkowski and K. Szalewicz, J. Chem. Phys. **133**, 094304 (2010).
[25] J. A. Barker, R. A. Fischer, and R. O. Watts, Mol. Phys. **21**, 657 (1971).
[26] J. A. Barker and A. Pompe, Aust. J. Chem. **21**, 1683 (1968).
[27] J. A. Barker, R. O. Watts, J. K. Lee, T. P. Schafer, and Y. T. Lee, J. Chem. Phys. **61**, 3081 (1974).
[28] G. Marcelli and R. J. Sadus, J. Chem. Phys. **111**, 1533 (1999).
[29] L. Wang and R. J. Sadus, J. Chem. Phys. **125**, 144509 (2006).
[30] L. Wang and R. J. Sadus, Phys. Rev. E **74**, 074503 (2006).
[31] M. Vlasiuk, F. Frascoli, and R. J. Sadus, J. Chem. Phys. **145**, 104501 (2016).
[32] B. M. Axilrod and E. Teller, J. Chem. Phys. **11**, 299 (1943).
[33] Y. Muto, J. Phys. Math. Soc. Japan **17**, 629 (1943).
[34] P. J. Leonard and J. A. Barker, in *Theoretical Chemistry: Advances and Perspectives*, edited by H. Eyring and D. Henderson (Academic, London, 1975), Vol. 1, p. 117.
[35] A. Z. Panagiotopoulos, N. Quirke, M. Stapleton, and D. J. Tildesley, Mol. Phys. **63**, 527 (1988).
[36] R. J. Sadus and J. M. Prausnitz, J. Chem. Phys. **104**, 4784 (1996).
[37] Đ. Plačkov and R. J. Sadus, Fluid Phase Equilib. **134**, 77 (1997).
[38] D. A. Kofke, J. Chem. Phys. **98**, 4149 (1993).
[39] W. Shi and J. K. Johnson, Fluid Phase Equilib. **187–188**, 171 (2001).
[40] M. Vlasiuk and R. J. Sadus, J. Chem. Phys. **147**, 024505 (2017).
[41] D. A. McQuarrie, *Statistical Mechanics* (Harper Collins, New York, 1976).